Journal of Computational Physics 229 (2010) 168–177

Contents lists available at ScienceDirect

Journal of Computational Physics

journal homepage: www.elsevier.com/locate/jcp

Cell-level canonical sampling by velocity scaling for multiparticle collision dynamics simulations

C.C. Huang [a], A. Chatterji [a,b], G. Sutmann [c], G. Gompper [a,d], R.G. Winkler [d,*]

[a] Institut für Festkörperforschung, Forschungszentrum Jülich, 52425 Jülich, Germany
[b] Indian Institute of Science Education and Research (IISER), Pune 411021, India
[c] Jülich Supercomputing Centre, Institute for Advanced Simulation, Forschungszentrum Jülich, 52425 Jülich, Germany
[d] Theoretical Soft-Matter and Biophysics, Institute for Advanced Simulation, Forschungszentrum Jülich, 2425 Jülich, Germany

ARTICLE INFO

Article history:
Received 27 May 2009
Received in revised form 18 September 2009
Accepted 22 September 2009
Available online 29 September 2009

PACS:
02.70.NS
05.20.Gg
61.20.Ja
61.20.Gy
83.50.Ax
47.60.Dx

Keywords:
Isothermal simulations
Canonical ensemble
Velocity scaling
Mesoscale hydrodynamics simulations
Multiparticle collision dynamics
Non-equilibrium simulations
Thermalization
Stochastic process

ABSTRACT

A local Maxwellian thermostat for the multiparticle collision dynamics algorithm is proposed. The algorithm is based on a scaling of the relative velocities of the fluid particles within a collision cell. The scaling factor is determined from the distribution of the kinetic energy within such a cell. Thereby the algorithm ensures that the distribution of the relative velocities is given by the Maxwell–Boltzmann distribution. The algorithm is particularly useful for non-equilibrium systems, where temperature has to be controlled locally. We perform various non-equilibrium simulations for fluids in shear and pressure-driven flow, which confirm the validity of the proposed simulation scheme. In addition, we determine the dynamic structure factors for fluids with and without thermostat, which exhibit significant differences due to suppression of the diffusive part of the energy transport of the isothermal system.

© 2009 Elsevier Inc. All rights reserved.

1. Introduction

Soft matter systems such as polymer and biopolymer solutions, colloidal suspensions, vesicles, cells, and microemulsions can display complex dynamical phenomena on the mesoscopic and macroscopic scale, which are governed by hydrodynamic interactions between their microscopic constituents. Direct simulation of such effects is difficult due to the presence of disparate length and time scales. The desire to bridge these scales stimulated the development of mesoscale simulation techniques. Among them, the multiparticle collision dynamics method (MPC) [1–4], a particle-based approach, proved well suited for hydrodynamic simulations in a broad spectrum of applications [5–12]. The algorithm consists of streaming and

* Corresponding author.
E-mail address: r.winkler@fz-juelich.de (R.G. Winkler).

0021-9991/$ - see front matter © 2009 Elsevier Inc. All rights reserved.
doi:10.1016/j.jcp.2009.09.024

collision steps. During the collisions, particles exchange momentum and energy. For a closed system, the algorithm conserves energy and momentum. In addition, the distribution function of a particle velocity is given by the Maxwell–Boltzmann distribution for a large number of particles in a system. However, this might no longer be true when the fluid is exposed to an external field, such as a shear or Poiseuille flow, because the additional forces lead to an increase of the kinetic energy of the fluid particles. In order to maintain a constant temperature, a control mechanisms has to be implemented.

Various constant temperature simulation schemes have been proposed in the literature [13–16,20–24,17,19,18,25]; not all of them ensure that a canonical ensemble is achieved. For molecular dynamics simulations of atomistic and molecular systems, the extended-phase-space method is very popular [13,14,23,24,17,19,18]. As has been shown, this method provides canonical ensemble averages when the system is chaotic [17,19,18]. Here, the phase space is typically extended by one or two additional variables, depending on its implementation. Hence, the additional numerical effort is small compared to the integration of the equations of motion for the large number of system degrees of freedom. The extended-phase-space method could also be applied to the MPC algorithm. However, in a study of the dynamics of dissolved particles in external fields, e.g., polymers, colloids, vesicles, etc., it is often necessary to control the temperature locally, because heat is generated non-homogeneously. This implies that a large number of additional variables would have to be introduced, which increases the numerical overhead. Moreover, the fluid particle equations of motion are more involved by the coupling to the heat bath degrees of freedom and a more sophisticated integration scheme is required compared to the analytical solution for the ballistic motion of the non-augmented fluid system.

Velocity scaling, as proposed in Refs. [16,26,4], leaves the equations of motion unchanged. In its simplest form, velocity scaling keeps the kinetic energy of a system at the desired value by multiplying the velocities of all particles by the same factor [8,27]. This corresponds to an isokinetic rather that an isothermal ensemble. The canonical kinetic energy distribution can be obtained by choosing a scale factor from the appropriate distribution of kinetic energies [16,26,4,25].

Various collision schemes have been proposed for the MPC algorithm [1,3,4,28,29]. Typically, the stochastic rotation dynamics (SRD) approach is adopted [1,3,4], which corresponds to a microcanonical ensemble. In SRD, temperature control can be achieved by either global, i.e., for all particles of a system, or local velocity rescaling. For an anisotropic and inhomogeneous system, global scaling might be inappropriate, because it would maintain temperature inhomogeneities. An elementary feature of MPC algorithms is the partition of fluid particles in collision cells. This aspect allows to set up a profile-unbiased thermostat [30,31,27] by subtracting the mean cell velocities from those of the individual particles of every cell and scaling of the relative velocities.

A canonical ensemble is simulated by the MPC scheme proposed in Refs. [28,29]. Here, in the collision step new relative velocities are assigned to every fluid particle, which are taken from a Maxwell–Boltzmann distribution. This approach is particular advantageous for simulations with angular momentum conservation [33,32].

Simulations are often performed applying periodic boundary conditions [13]. Excess heat produced by an external field cannot be removed in this case via any physical mechanism such as walls. Thus, it is necessary to apply one or the other of the described thermostats. A fluid system confined between surfaces could be thermalized by connecting the surfaces to a heat reservoir [34]. The extent to which heat is taken out of the system then depends on the heat-conducting properties of the model fluid [34]. For a reasonably realistic model of a fluid, we would not want to perturb the system by an additional thermostat. The situation may be different for a model fluid, where heat conduction may perturb the desired description of the fluid. Since we are typically interested in a solution of Stokes equation with a homogeneous temperature, an additional local temperature control is necessary even for a system confined between walls.

In this article, we propose an alternative velocity-scaling method. Instead of sampling the scale factor from the Maxwell–Boltzmann distribution of the velocities by a Monte Carlo scheme [16,26,4], we take the kinetic energy directly from its thermal distribution function. Hence, we assure that the scaling factor obeys the correct distribution and statistical properties such as detailed balance are correctly captured, in contrast to Monte Carlo procedures for rescaling velocities [26,4]. For this purpose, we will first determine the distribution function of the kinetic energy of our system. By applying the method to fluid simulations under shear, we demonstrate that even the local velocities obey the Maxwell–Boltzmann distribution. In a study of a fluid confined between two parallel walls, which is exposed to a pressure gradient, we demonstrate the inability of the global scaling scheme to yield the correct velocity profile, temperature, and particle density distribution. At the same time, the newly proposed scaling scheme provides the desired fluid behavior.

The article is organized as follows. In Section 2, the multiparticle collision dynamics method as well our cell-level Maxwellian thermostat are described. Results for the fluid velocity distributions in the presence of shear and Poiseuille flows are presented in Section 3. Differences in the dynamic structure factors of thermalized and non-thermalized MPC fluids are discussed in Section 4. Section 5 summarizes our results.

2. The model

2.1. Multiparticle collision dynamics

In the MPC algorithm, the fluid is modeled by a set of N point-like particles of mass m each, which move in continuous space with velocities determined by a stochastic process. The algorithm consists of alternating streaming and collision steps [1]. In the streaming step, the particles move ballistically and their positions are updated according to

$$\boldsymbol{r}_i(t+\Delta t) = \boldsymbol{r}_i(t) + \boldsymbol{v}_i(t)\Delta t, \tag{1}$$

where $\boldsymbol{r}_i(t)$ denotes the position of particle i at time t, $\boldsymbol{v}_i(t)$ its velocity, and Δt the time interval between two collisions, which we term collision time.

The streaming step is followed by a collision step in which the particles interact with each other and exchange momentum. In three-dimensions, the simulation box is partitioned into cubic collision cells of side length a. For the SRD version of MPC [4], the relative velocities with respect to the center-of-mass velocity $\boldsymbol{v}_{cm}$ of every cell are rotated by an angle α according to

$$\boldsymbol{v}_i(t+\Delta t) = \hat{\boldsymbol{v}}_{cm}(t) + \mathbf{R}(\alpha)[\hat{\boldsymbol{v}}_i(t+\Delta t) - \hat{\boldsymbol{v}}_{cm}(t+\Delta t)], \tag{2}$$

where $\hat{\boldsymbol{v}}_i(t+\Delta t) = \boldsymbol{v}_i(t)$ is the velocity after streaming and $\mathbf{R}(\alpha)$ the rotation matrix. The orientation of the rotation axis is chosen randomly for every collision cell and time step. The rotation matrix reads

$$\mathbf{R}(\alpha) = \begin{pmatrix} l_x^2 + (1-l_x^2)c & l_x l_y(1-c) - l_z s & l_x l_z(1-c) + l_y s \\ l_x l_y(1-c) + l_z s & l_y^2 + (1-l_y^2)c & l_y l_z(1-c) - l_x s \\ l_x l_z(1-c) - l_y s & l_y l_z(1-c) + l_x s & l_z^2 + (1-l_z^2)c \end{pmatrix},$$

with $l_x = \cos(\varphi)\sqrt{1-\theta^2}, l_y = \sin(\varphi)\sqrt{1-\theta^2}, l_z = \theta, c = \cos(\alpha)$, and $s = \sin(\alpha)$. φ and θ are uncorrelated random numbers, which are taken from uniform distributions in the intervals $[0, 2\pi]$ and $[-1, 1]$, respectively. The conservation of mass, momentum, and energy in a collision step leads to long-range correlations between the particles [1,2]. The velocity distribution satisfies the Maxwell–Boltzmann distribution in the limit $N \to \infty$ [3] and the probability to find N_c particles in a cell is given by the Poisson distribution

$$p(N_c) = e^{-\langle N_c\rangle}\langle N_c\rangle^{N_c}/N_c!, \tag{3}$$

where $\langle N_c\rangle$ is the average number of the particles found in a cell. As has been shown, this dynamics yields the correct hydrodynamic behavior [3,4,35,36]. Notice that the presence of an external field, such as shear flow or a gravitational field, the velocity changes during the streaming step [38,39,11,12,37], i.e., $\hat{\boldsymbol{v}}_i(t+\Delta t) \neq \boldsymbol{v}_i(t)$. To ensure Galilean invariance, a random shift of the collision cells is performed in every collision step [40].

2.2. Cell-level canonical thermostat

The velocity distribution function for a system of N_c fluid particles of an isothermal system is given by the Maxwell–Boltzmann distribution

$$P(\{\boldsymbol{v}\}) = \left(\frac{m}{2\pi k_B T}\right)^{3N_c/2} \exp\left(-\frac{m}{2k_B T}\sum_{i=1}^{N_c}\boldsymbol{v}_i^2\right), \tag{4}$$

where k_B is the Boltzmann constant and T the temperature. The distribution function for the (local) kinetic energy $E_k = (m/2)\sum_{i=1}^{N_c}\Delta\boldsymbol{v}_i^2$ is obtained from the relation

$$P(E_k) = \frac{1}{Z}\int \delta\left(E_k - \frac{m}{2}\sum_{i=1}^{N_c}\Delta\boldsymbol{v}_i^2\right)\delta\left(\sum_{i=1}^{N_c}\Delta\boldsymbol{v}_i\right)\exp\left(-\frac{m}{2k_B T}\sum_{i=1}^{N_c}\Delta\boldsymbol{v}_i^2\right)d^{N_c}\Delta\boldsymbol{v}, \tag{5}$$

with the partition function $Z = \int \delta\left(\sum_{i=1}^{N_c}\Delta\boldsymbol{v}_i\right)\exp\left(-\frac{m}{2k_B T}\sum_{i=1}^{N_c}\Delta\boldsymbol{v}_i^2\right)d^{N_c}\Delta\boldsymbol{v}$. Note, in the presence of an external field, only the relative velocities $\Delta\boldsymbol{v}_i = \boldsymbol{v}_i - \boldsymbol{v}_{cm}$ obey the Maxwell–Boltzmann distribution. This is taken into account by the δ-function with the sum of the velocities. Evaluation of the integrals yields [25]

$$P(E_k) = \frac{1}{E_k\Gamma(f/2)}\left(\frac{E_k}{k_B T}\right)^{f/2}\exp\left(-\frac{E_k}{k_B T}\right). \tag{6}$$

Here, $f = 3(N_c - 1)$ denotes the degrees of freedom of the system and $\Gamma(x)$ is the gamma function. The distribution function $P(E_k)$ itself is denoted as gamma distribution. In the limit $f \to \infty$, the gamma distribution turns into a Gaussian function with the mean $\langle E_k\rangle = f k_B T/2$ and variance $f(k_B T)^2/2$.

To thermalize the velocities of the MPC fluid on the cell level, an energy E_k' is taken from the distribution function (6) for every cell and time step and the velocities $\Delta\boldsymbol{v}_i$ of the particles within a cell are scaled by the corresponding factor α, i.e, $\Delta\boldsymbol{v}_i' = \alpha\Delta\boldsymbol{v}_i$, with

$$\alpha = \left(\frac{2E_k'}{m\sum_{i=1}^{N_c}\Delta\boldsymbol{v}_i^2}\right)^{1/2}. \tag{7}$$

For fixed N_c, we then obtain the following distribution function for the relative velocity of a particle in a cell in the limit of a large number of MPC steps

$$P(\Delta\boldsymbol{v}, N_c) = \left(\frac{m}{2\pi k_B T(1-1/N_c)}\right)^{3/2}\exp\left(-\frac{m}{2k_B T(1-1/N_c)}\Delta\boldsymbol{v}^2\right). \tag{8}$$

However, the number of fluid particles in a cell is fluctuating in time. Thus, the actual distribution function is obtained by averaging Eq. (8) over the Poisson distribution (3)

$$P(\Delta\boldsymbol{v}) = \sum_{N_c=2}^{\infty} e^{-\langle N_c\rangle} \frac{\langle N_c\rangle^{N_c}}{N_c!} P(\Delta\boldsymbol{v}, N_c) / \left(1 - (\langle N_c\rangle + 1)e^{-\langle N_c\rangle}\right). \tag{9}$$

In the following, we will denote this type of temperature control as Maxwell–Boltzmann-scaling (MBS) thermostat.

3. Test of the thermostat

We performed various simulations of an MPC fluid to demonstrate the suitability of the proposed thermalization procedure. Since we expect a severe dependence of the velocity distribution on the applied thermostat for non-equilibrium systems only, we will focus on results for fluids exposed to shear flow and Poiseuille flow. The validity of the thermostat is evaluated by considering the velocity distribution on the cell level, the temperature profile, and the density profile. The energies E_k' for the velocity scaling (7) are determined by the gamma function distribution of the NAG library [41].

3.1. Shear flow

For the shear-flow simulations, we consider a system with a cubic simulation box of side length $L = 30a$ and periodic boundary conditions. Systems with the average particle numbers $\langle N_c\rangle = 3, 5$, and 10 are considered, corresponding to values typically used in simulations [3,4]. Lengths and time are scaled according to $\tilde{r}_\beta = r_\beta/a$, with $\beta \in \{x, y, z\}$, and $\tilde{t} = t\sqrt{k_BT/ma^2}$, which corresponds to the choice $k_BT = 1, a = 1$, and $m = 1$. The rotation angle is set to $\alpha = 130^o$ and the collision time to $\Delta\tilde{t} = 0.1$. This corresponds to a fluid system, where the transport of momentum is mainly due to collisions [35,42]. A stationary and homogeneous shear flow is established by applying Lees–Edwards boundary conditions [43] with flow along the x-axis and the gradient along the y-axis. To test the thermostat under strong shear flow, the shear rate is chosen as $\tilde{\dot{\gamma}} = 0.3$.

The simulation results show that the MBS thermostat efficiently controls the local, and hence global, temperature in a profile-unbiased way. Fig. 1 displays results for the distribution of the magnitude of the particle velocities within the collision cells for various particle numbers. The comparison with the corresponding theoretical expression Eq. (9) exhibits excellent agreement and confirms that the MBS thermostat yields the correct local velocity distribution under strong shear flow. The shift of the curves for the various particle numbers shows the strong dependence of the distribution on the particle number fluctuations in a collision cell. Naturally, this effect disappears with increasing particle number and a limiting curve is assumed for $\langle N_c\rangle \to \infty$.

For comparison, the inset of Fig. 1 shows the velocity distribution obtained by scaling the relative velocities according to

$$\Delta\boldsymbol{v}_i' = \Delta\boldsymbol{v}_i \sqrt{\frac{3(N_c - 1)k_BT}{m\sum_{i=1}^{N_c}\Delta\boldsymbol{v}_i^2}}. \tag{10}$$

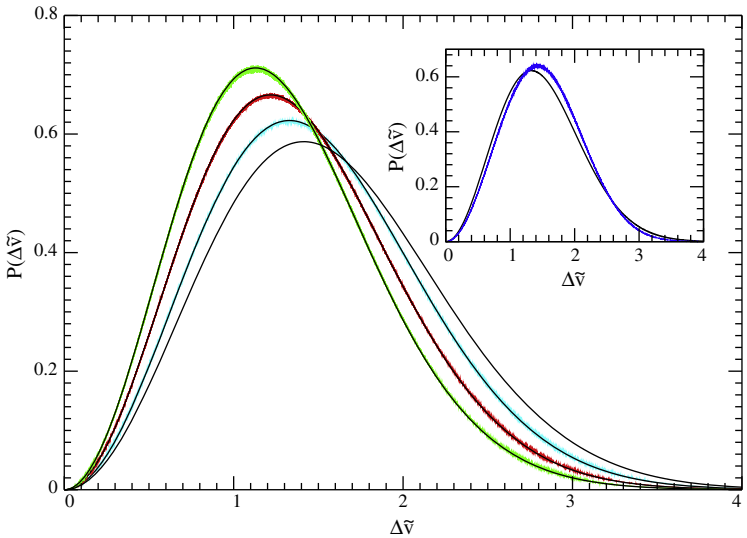

Fig. 1. Distribution functions of the particle velocities $|\Delta\boldsymbol{v}|$ in a collision cell under shear flow for the average particle numbers $\langle N_c\rangle = 3, 5, 10$, and ∞ (left to right). The solid lines are determined using Eq. (9). The inset shows the distribution function for velocity scaling with the average kinetic energy according to Eq. (10) for $\langle N_c\rangle = 10$ in comparison to the correct Maxwell–Boltzmann result (smooth line).

This is a straightforward extension of the profile-unbiased velocity-scaling method to the collision-cell level [27,30,31]. The thermostat yields the correct local temperature, however the velocity distribution function is clearly different from that expected theoretically (Eq. (9)). This emphasizes the relevance of the fluctuations in the kinetic energy to arrive at the correct canonical distribution.

3.2. Poiseuille flow

In the Poiseuille flow simulations, the MPC fluid is confined between two planar walls parallel to the *xz*-plane of the reference system and periodic boundary conditions are applied parallel to the walls [38,28,7,11]. A gravitational field acting on every fluid particle induces a flow along the *x*-axis corresponding to a pressure-driven flow. Hence, the streaming step of the MPC algorithm along the flow direction is now given by

$$\hat{v}_{ix}(t+\Delta t) = v_{ix}(t) + g\Delta t, \tag{11}$$

$$r_{ix}(t+\Delta t) = r_{ix}(t) + v_{ix}(t)\Delta t + \frac{1}{2}g\Delta t^2. \tag{12}$$

Applying the bounce-back rule [38] to account for the no-slip boundary conditions leads to a parabolic velocity profile

$$v_x(y) = \frac{4v_{max}(H-y)y}{H^2} \tag{13}$$

in the stationary state, where H is the distance between the two walls and v_{max} is the maximum flow velocity. The velocity v_{max} depends on the strength of the applied field, the surface separation, and the viscosity η of the fluid [44]

$$v_{max} = \frac{mN_c g H^2}{8\eta}. \tag{14}$$

To reduce fluid slip at the surfaces, the phantom-particle approach is adopted as proposed in Ref. [38] with the extension described in Ref. [37] to account for particle number fluctuations. This means that the collision cells penetrated by walls and hence containing a smaller number of particles than bulk cells are filled with phantom particles. As number of phantom particles, we choose the number of (real) particles contained in the surface cells at the opposite wall and intercepted by this wall. The velocity of the phantom particles is taken from the Maxwell–Boltzmann distribution. Since the sum of Gaussian random numbers is again Gaussian, it suffices to determine a single random vector $\boldsymbol{P}$ from a Gaussian distribution function with zero mean and variance $mN_p k_B T$, where N_p is the number of phantom particles. The center-of-mass velocity of the surface cell with phantom particles is then given by $\hat{\boldsymbol{v}}_{cm} = \left(\sum_{i=1}^{N_c}\hat{\boldsymbol{v}}_i + \boldsymbol{P}\right)/(N_c+N_p)$. In the collision step, the relative velocities with respect to $\hat{\boldsymbol{v}}_{cm}$ of the particles within this cell are rotated.

The same parameters as for the shear-flow simulations are used, except for the system size which is $L_x = L_z = H = 20a$. The gravitational field strength is $\tilde{g} = 0.01$.

For comparison, additional simulations are performed without any thermostat and with a profile-unbiased global scaling scheme. In the latter case, the velocities are scaled according to

$$\Delta\boldsymbol{v}_i' = \Delta\boldsymbol{v}_i\sqrt{\frac{3(N-N_{cl})k_BT}{m\sum_{i=1}^{N}\Delta\boldsymbol{v}_i^2}}, \tag{15}$$

where N_{cl} is the number of cells occupied by particles [27]. In contrast to Eq. (10), all fluid particles are taken into account to calculate the scaling factor and all particles are scaled by the same factor. Hence, we will denote this scheme as global scaling in the following.

The measured velocity profiles for the three different thermalization schemes are shown in Fig. 2(a). All of them yield parabolic velocity profiles with a similar small but finite slip at the walls. This slip is a consequence of the non-local interaction between the fluid particles in the collision step. However, the slip is not affecting the viscosity of the fluid. Simply a larger value of H, determined by extrapolating the profile to $v_x = 0$, has to be used in Eq. (13) to determine the viscosity from this expression. The figure reflects the influence of the thermostat on the velocity profile. The viscosity extracted from the profile via Eqs. (13) and (14) is $\tilde{\eta} = 8.7$ for the MBS thermostat, in agreement with theoretical expectations [37], while thermalization by collisions with wall phantom particles yields a 3% larger and by global scaling a 5% smaller value. The reason for the differences is evident from Fig. 2(b and c), which show the profiles for the normalized kinetic energy $\widetilde{E}_k = 2E_k/(3k_BT)$ and particle number. The external field increases the kinetic energy and hence the temperature of the MPC particles. Without explicit thermostat, the system is thermalized by the wall phantom particles. Evidently, the heat transport within the fluid is not fast enough to ensure a constant kinetic energy across the slit. A stationary state is reached, where the temperature is close to the desired value at the walls, but is larger in the central part of the slit [34]. A similar inhomogeneity, although less pronounced, has been found in Ref. [45] in dissipative particle dynamics (DPD) simulations of periodic Poiseuille flows. Accompanied by kinetic energy inhomogeneities are variations in the particle number in a collision cell. For a lower temperature a larger particle density is obtained and vice versa. Global scaling restores the average kinetic energy of the system, however, the local kinetic energy is not uniform across the slit. Again, the kinetic energy modulation is accompanied by density inhomogeneities. Only the MBS thermostat ensures uniform kinetic energy and density profiles across the slit.

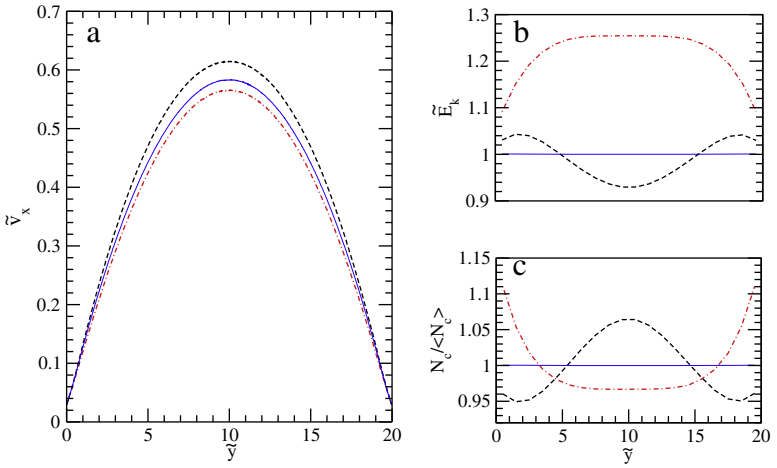

Fig. 2. Velocity (a), kinetic energy (b), and particle density profiles (c) for a fluid without explicit thermostat (dashed-dotted), the MBS thermostat (solid), and global scaling (dashed).

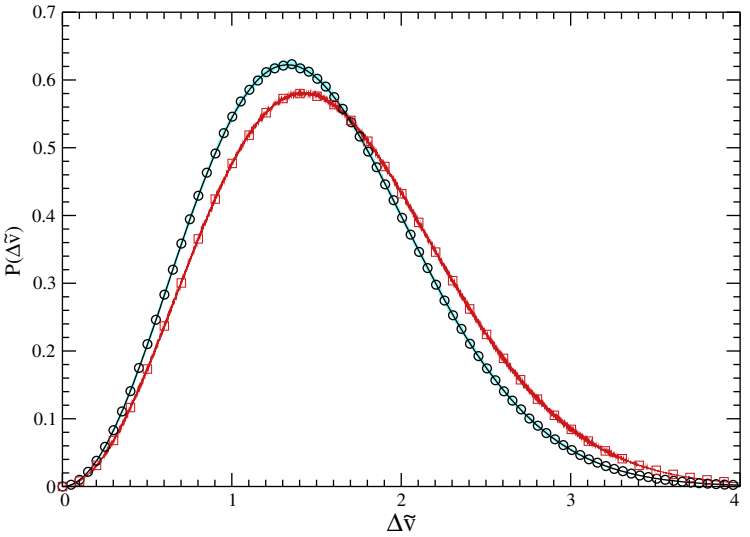

Fig. 3. Distribution functions of the particle velocities $|\Delta \boldsymbol{v}|$ in a collision cell for a Poiseuille flow. Results are displayed for a systems with global scaling (circles), an MBS thermostat (solid line under circles), and without explicit thermostat (solid line with squares). The distribution function obtained from the theoretical expression (9) (black line) is hardly distinguishable from the simulation results with MBS thermostat.

As for the shear-flow simulations, the velocity distribution for the MBS thermostat agrees with the theoretical expression Eq. (9) (cf. Fig. 3). In addition, the distribution function of the particle velocities in a collision cell obtained by the global scaling scheme agrees very well with the theoretical expression despite the modulations in the temperature profile. The origin lies on the one hand in the large number of particles involved in global temperature scaling. With increasing number of degrees of freedom, the effect of velocity scaling on the distribution function becomes smaller and vanishes in the limit of infinitely many degrees of freedom. On the other hand, our calculations of the velocity distribution functions in the regions of higher, i.e., $0 < \tilde{y} < 5$ and $15 < \tilde{y} < 20$, and lower, i.e., $5 < \tilde{y} < 15$, kinetic energies yield distributions which are shifted to lower and higher velocities, respectively, compared to the MBS distribution. This demonstrates the influence of the modified kinetic energies on the velocity distribution. However, the distribution determined over the whole system is indistinguishable from the MBS distribution within the accuracy of the simulation, because the shifts cancel to leading order in $\Delta E_k/E_k$. In contrast, for the system without explicit scaling, the velocity distribution function is shifted to larger velocities and broadened due to the higher mean temperature.

4. Dynamic structure factor

Thermal fluctuations of the particle density $\rho(\boldsymbol{r}, t)$ are dynamically coupled and the analysis of their dynamic correlation functions in the limit of small wave vectors and frequencies provides insight into the transport coefficients of the fluid [46,4].

The dynamic structure factor is easily accessible by scattering techniques and, thus, is widely used to determine dynamic and transport coefficients of fluids [47]. To illustrate the differences between a non-thermalized equilibrium system and the system with an MBS thermostat, we determine the dynamic structure factor of the MPC fluid.

The dynamic structure factor is defined as [48]

$$S(\boldsymbol{k},\omega) = \int \langle \rho(\boldsymbol{k},t)\rho(-\boldsymbol{k},0)\rangle e^{-i\omega t}\,dt, \tag{16}$$

with the intermediate scattering function $F(\boldsymbol{k},t) = \langle \rho(\boldsymbol{k},t)\rho(-\boldsymbol{k},0)\rangle$ and the density of our point-like particles in Fourier space

$$\rho(\boldsymbol{k},t) = \frac{1}{\sqrt{N}} \sum_{j=1}^{N} e^{i\boldsymbol{k}\boldsymbol{r}_j(t)}. \tag{17}$$

Evaluation of the expressions yields [46]

$$S(\boldsymbol{k},\omega) = k_B T N_c \left\{ \left(\frac{c_v}{c_p}\right) \frac{c^2 k^4 \Gamma}{(\omega^2 - c^2k^2)^2 + (\omega k^2 \Gamma)^2} + \left(1 - \frac{c_v}{c_p}\right) \frac{D_T k^2}{\omega^2 + (k^2 D_T)^2} - \left(1 - \frac{c_v}{c_p}\right) \frac{(\omega^2 - c^2k^2) D_T k^2}{(\omega^2 - c^2k^2)^2 + (\omega k^2 \Gamma)^2} \right\} \tag{18}$$

for a system without thermostat. Here, D_T is the thermal diffusion coefficient, Γ the sound attenuation factor, c_v and c_p are the specific heat capacities at constant volume and pressure, respectively, and c is the adiabatic speed of sound. The definitions of the individual terms are given in the appendix.

To investigate the effect of a local thermostat, we perform simulations for a cubic simulation box of side length $L = 20a$ with periodic boundary conditions. The other parameters are the same as for the simulation of the Poiseuille flow. Velocity scaling via the MBS thermostat is performed at every collision step.

Fig. 4 displays simulation results with and without temperature scaling for the smallest wave vector $k = 2\pi/L$. Evidently, the theoretical expression (18) agrees very well with the simulation result without thermostat. The dynamic structure factor for the thermalized system differs significantly from that of the non-thermalized system: The central peak completely vanishes and the Brillouin peaks are shifted to frequencies of smaller magnitude (cf. Fig. 4). As Fig. 5 shows, the exponential decay in the time correlation function $F(\boldsymbol{k},t)$ is absent for the MBS scheme, which translates into a missing central peak in the spectra which in turn is related to thermal diffusion. The differences in $S(\boldsymbol{k},\omega)$ are explained as follows: The local thermostat controls the temperature on the length scale of a collision cell. The velocities of all particles within a given cell obey the correct energy distribution function. Hence, there is no diffusive energy transport. Energy is transported only via sound waves, which is manifested in the presence of the Brillouin peaks. Furthermore, a local thermostat maintains a homogenous distribution of kinetic energy on a microscopic scale and therefore corresponds to an isothermal rather than an adiabatic situation. As a consequence, the sound propagation should exhibit an isothermal sound velocity c_T rather than an adiabatic sound velocity c_S, where

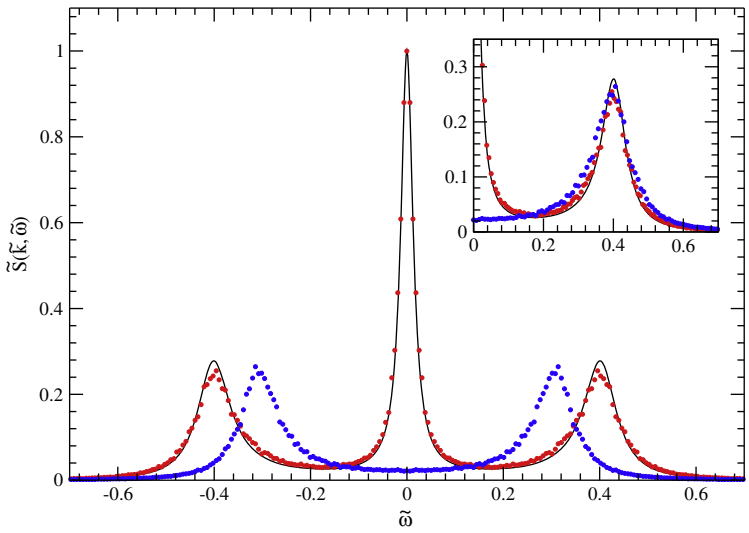

Fig. 4. Dynamic structure factor for $k = 2\pi/L$ for a system without thermalization (data with central peak) and with the MBS thermostat (data without central peak), respectively. The solid line is calculated according to Eq. (18). In the inset, the frequency scale for the isothermal structure factor has been multiplied by $\sqrt{c_p/c_v} = \sqrt{5/3}$.

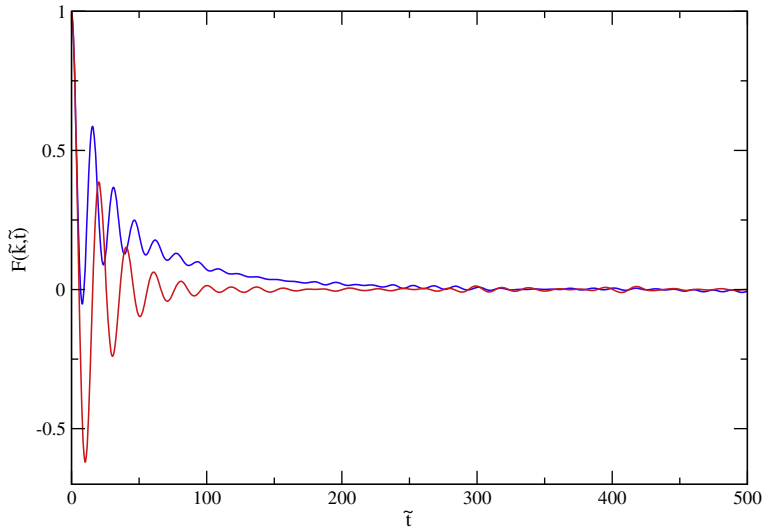

Fig. 5. Intermediate scattering function ($k = 2\pi/L$) for an MPC fluid without thermostat (top) and with the MBS thermostat (bottom), respectively.

$$c_S = \sqrt{\gamma} c_T = \sqrt{\frac{\gamma k_B T}{m}} \tag{19}$$

for the MPC fluid. This is confirmed by the simulation. The frequency $\omega_B(k)$ of the Brillouin peak is connected with the generalized sound velocity by the dispersion relation

$$\omega_B(k) = c_T(k) k. \tag{20}$$

Hence, it is clear that the frequencies of the Brillouin peaks for the two types of simulations should be shifted by a factor $\sqrt{c_p/c_v} = \sqrt{5/3}$. The comparison of the Brillouin frequencies of Fig. 4 confirms that this indeed applies.

5. Conclusions

We have introduced a cell-level thermostat for the SRD version of MPC dynamics, which yields a Maxwell–Boltzmann distribution for the fluid particle velocities. In the MBS thermostat, the relative velocities with respect to the center-of-mass velocity of a collision cell of all particles within such cell are scaled by a stochastic factor, leaving the dynamical properties of the system unaltered. The stochastic factor is determined from the distribution function (gamma distribution) of the kinetic energy of the fluid particles. The comparison of the simulation results with theoretical expected distribution functions shows that the MBS method produces the desired behavior on a local scale.

The MBS thermostat roughly increases the amount of required CPU time by 70% compared to a non-thermalized system. A slightly smaller increase in CPU time is obtained for the local velocity-scaling scheme according to Eq. (10). In both cases, the additional CPU time is spend for the calculation of the kinetic energy and the scaling of the velocities. The MPC algorithm assigning Maxwellian distributed random relative velocities in the collision step requires approximately 20% more CPU time [28,27] for a three-dimensional system as the MBS method, as our tests have been shown. Hence, the various thermostats increase the required CPU time by approximately the same amount. For moderate external fields, thermalization is not required at every MPC step. Thus, the additional CPU load can be reduced if the kinetic energy is adjusted every few MPC steps only.

We like to point out that the MBS thermalization method can also be applied to other particle simulation methods. For example, in a standard molecular dynamics simulation [25], the velocities of all particles can be scaled using the factor α of Eq. (7), where the sum is over all particles, to arrive at a Maxwellian velocity distribution.

Acknowledgement

Financial support of this work by the German Research Foundation (DFG) within SFB TR 6 "Physics of Colloidal Dispersions in External Fields" is gratefully acknowledged.

Appendix A. Definitions

In this appendix the various variables defined in Section 4 are given in terms of the MPC fluid parameters [46].
The thermal diffusion coefficient D_T reads

$$D_T = D_{T,col} + D_{T,kin}, \tag{21}$$

with

$$D_{T,col} = \frac{a^2}{\Delta t}\left(1 - \frac{1}{\langle N_c\rangle}\right)\frac{1-\cos\alpha}{15\langle N_c\rangle}, \tag{22}$$

$$D_{T,kin} = \frac{1}{2}\frac{k_B T}{m}\Delta t\left(\frac{3}{1-\cos\alpha} - 1 + \frac{6}{\langle N_c\rangle}\left(\frac{4}{5} - \frac{1}{4}\frac{1}{\sin^2\alpha/2}\right)\right). \tag{23}$$

The specific heat capacities are given by

$$c_v = \frac{3k_B}{2m}, \quad c_p = c_v + \frac{k_B}{m}, \quad \gamma = \frac{c_p}{c_v} = \frac{5}{3}. \tag{24}$$

The sound attenuation factor is defined as

$$\Gamma = D_T(\gamma - 1) + D_v, \tag{25}$$

with

$$D_v = \frac{4}{3}(v_{kin} + v_{col}) \tag{26}$$

and the kinematic viscosity

$$v = v_{kin} + v_{col}, \tag{27}$$

where

$$v_{kin} = \frac{k_B T}{2m}\Delta t\left(\frac{5\langle N_c\rangle}{(\langle N_c\rangle - 1 + e^{-\langle N_c\rangle})(2 - \cos\alpha - \cos 2\alpha)} - 1\right), \tag{28}$$

$$v_{col} = \frac{a^2}{18\langle N_c\rangle\Delta t}(\langle N_c\rangle - 1 + e^{-\langle N_c\rangle})(1 - \cos\alpha). \tag{29}$$

References

[1] A. Malevanets, R. Kapral, Mesoscopic model for solvent dynamics, J. Chem. Phys. 110 (1999) 8605–8613.
[2] A. Malevanets, R. Kapral, Solute molecular dynamics in a mesoscopic solvent, J. Chem. Phys. 112 (2000) 7260–7269.
[3] R. Kapral, Multiparticle collision dynamics: simulation of complex systems on mesoscales, Adv. Chem. Phys. 140 (2008) 89.
[4] G. Gompper, T. Ihle, D.M. Kroll, R.G. Winkler, Multi-particle collision dynamics – a particle based mesoscale simulation approach to the hydrodynamics of complex fluids, Adv. Polym. Sci. 221 (2009) 1.
[5] J.T. Padding, A.A. Louis, Hydrodynamic and Brownian fluctuations in sedimenting suspensions, Phys. Rev. Lett. 93 (2004) 220601.
[6] N. Kikuchi, J.F. Ryder, C.M. Pooley, J.M. Yeomans, Kinetics of the polymer collapse transition: the role of hydrodynamics, Phys. Rev. E 71 (2005) 061804.
[7] H. Noguchi, G. Gompper, Shape transitions of fluid vesicles and red blood cells in capillary flow, Proc. Natl. Acad. Sci. USA 102 (2005) 14159–14164.
[8] M. Ripoll, R.G. Winkler, G. Gompper, Star polymers in shear flow, Phys. Rev. Lett. 96 (2006) 188302.
[9] J.F. Ryder, J.M. Yeomans, Shear thinning in dilute polymer solutions, J. Chem. Phys. 125 (2006) 194906.
[10] Y.-G. Tao, I.O. Götze, G. Gompper, Multiparticle collision dynamics modeling of viscoelastic fluids, J. Chem. Phys. 128 (2008) 144902.
[11] L. Cannavacciuolo, R.G. Winkler, G. Gompper, Mesoscale simulations of polymer dynamics in microchannel flow, EPL 83 (2008) 38007.
[12] S. Frank, R.G. Winkler, Polyelectrolyte electrophoresis: field effects and hydrodynamic interactions, EPL 83 (2008) 38004.
[13] M.P. Allen, D.J. Tildesley, Computer Simulation of Liquids, Clarendon Press, Oxford, 1987.
[14] D. Frenkel, B. Smit, Understanding Molecular Simulation, Academic, New York, 2002.
[15] H.C. Andersen, Molecular dynamics simulations at constant pressure and/or temperature, J. Chem. Phys. 72 (1980) 2384.
[16] D.M. Heyes, Molecular dynamics at constant pressure and temperature, Chem. Phys. 82 (1983) 285.
[17] A. Bulgac, D. Kusnezov, Canonical ensemble averages from pseudo microcanonical dynamics, Phys. Rev. A 42 (1990) 5045.
[18] R.G. Winkler, V. Kraus, P. Reineker, Time reversible and phase-space conserving molecular dynamics at constant temperature, J. Chem. Phys. 102 (1995) 9018.
[19] R.G. Winkler, Extended-phase-space isothermal molecular dynamics: canonical harmonic oscillator, Phys. Rev. A 45 (1992) 2250.
[20] J.M. Haile, S. Gupta, Extension of the molecular dynamics simulation method. II. Isothermal systems, J. Chem. Phys. 79 (1983) 3067.
[21] H.J.C. Berendsen, J.P.M. Postma, W.F. van Gunsteren, A. DiNola, J.R. Haak, Molecular dynamics with coupling to an external bath, J. Chem. Phys. 81 (1984) 3684.
[22] D.J. Evans, G.P. Morriss, Non-Newtonian molecular dynamics, Comput. Phys. Rep. 1 (1984) 297.
[23] S. Nosé, A unified formulation of the constant temperature molecular dynamics methods, J. Chem. Phys. 81 (1984) 511.
[24] W.G. Hoover, Canonical dynamics: equilibrium phase-space distributions, Phys. Rev. A 31 (1985) 1695.
[25] G. Bussi, D. Donadio, M. Parrinello, Canonical sampling through velocity scaling, J. Chem. Phys. 126 (2007) 014101.
[26] M. Hecht, J. Hartin, T. Ihle, H.J. Herrmann, Simulation of claylike colloids, Phys. Rev. E 72 (2005) 011408.
[27] H. Noguchi, G. Gompper, Transport coefficients of dissipative particle dynamics with finite time step, EPL 79 (2007) 36002.
[28] E. Allahyarov, G. Gompper, Mesoscopic solvent simulations: multiparticle-collision dynamics of three-dimensional flows, Phys. Rev. E 66 (2002) 036702.
[29] H. Noguchi, N. Kikuchi, G. Gompper, Particle-based mesoscale hydrodynamic techniques, EPL 78 (2007) 10005.
[30] D.J. Evans, G.P. Morriss, Shear thickening and turbulence in simple fluids, Phys. Rev. Lett. 56 (1986) 2172.
[31] D.J. Evans, G.P. Morriss, Statistical Mechanics of Nonequilibrium Liquids, Academic Press, London, 1990.
[32] H. Noguchi, G. Gompper, Transport coefficients of off-lattice mesoscale-hydrodynamics simulation techniques, Phys. Rev. E 78 (2008) 016706.
[33] I.O. Götze, H. Noguchi, G. Gompper, Relevance of angular momentum conservation in mesoscale hydrodynamics simulations, Phys. Rev. E 76 (2007) 046705.

[34] B.D. Todd, D.J. Evans, Temperature profile for poiseuille flow, Phys. Rev. E 55 (1997) 2800.
[35] M. Ripoll, K. Mussawisade, R.G. Winkler, G. Gompper, Low-Reynolds-number hydrodynamics of complex fluids by multi-particle-collision dynamics, Europhys. Lett. 68 (2004) 106.
[36] K. Mussawisade, M. Ripoll, R.G. Winkler, G. Gompper, Dynamics of polymers in a particle based mesoscopic solvent, J. Chem. Phys. 123 (2005) 144905.
[37] R.G. Winkler, C.-C. Huang, Stress tensors of multiparticle collision dynamics fluids, J. Chem. Phys. 130 (2009) 074907.
[38] A. Lamura, G. Gompper, T. Ihle, D.M. Kroll, Multiparticle collision dynamics: flow around a circular and a square cylinder, Europhys. Lett. 56 (2001) 319–325.
[39] A. Lamura, G. Gompper, Numerical study of the flow around a cylinder using multi-particle collision dynamics, Eur. Phys. J. E 9 (2002) 477–485.
[40] T. Ihle, D.M. Kroll, Stochastic rotation dynamics: a Galilean-invariant mesoscopic model for fluid flow, Phys. Rev. E 63 (2001) 020201(R).
[41] <http://www.nag.co.uk>.
[42] M. Ripoll, K. Mussawisade, R.G. Winkler, G. Gompper, Dynamic regimes of fluids simulated by multi-particle-collision dynamics, Phys. Rev. E 72 (2005) 016701.
[43] A.W. Lees, S.F. Edwards, The computer study of transport under extreme conditions, J. Phys. C: Solid State Phys. 5 (1972) 1921.
[44] D.J. Tritton, Physical Fluid Dynamics, Oxford University Press, Oxford, 1988.
[45] J.A. Backer, C.P. Lowe, H.C.J. Hoefsloot, P.D. Iedema, Poiseuille flow to measure the viscosity of particle model fluids, J. Chem. Phys. 122 (2005) 154503.
[46] E. Tüzel, T. Ihle, D.M. Kroll, Dynamic correlations in stochastic rotation dynamics, Phys. Rev. E 74 (2006) 056701.
[47] B.J. Berne, R. Pecora, Dynamic Light Scattering: With Applications to Chemistry, Biology, and Physics, Wiley, New York, 1976.
[48] J.-P. Hansen, I.R. McDonald, Theory of Simple Liquids, Academic Press, London, 1986.